

Multifunctional nanorods for gene delivery

ALIASGER K. SALEM^{1,2}, PETER C. SEARSON² AND KAM W. LEONG*¹¹Department of Biomedical Engineering, Johns Hopkins School of Medicine, Baltimore, Maryland 21205, USA²Department of Materials Science and Engineering, Johns Hopkins University, Baltimore, Maryland 21218, USA

*e-mail: kleong@bme.jhu.edu

Published online: 14 September 2003; doi:10.1038/nmat974

The goal of gene therapy is to introduce foreign genes into somatic cells to supplement defective genes or provide additional biological functions^{1,2}, and can be achieved using either viral or synthetic non-viral delivery systems. Compared with viral vectors, synthetic gene-delivery systems, such as liposomes and polymers, offer several advantages including ease of production and reduced risk of cytotoxicity and immunogenicity^{3,4}, but their use has been limited by the relatively low transfection efficiency. This problem mainly stems from the difficulty in controlling their properties at the nanoscale. Synthetic inorganic gene carriers have received limited attention in the gene-therapy community, the only notable example being gold nanoparticles with surface-immobilized DNA applied to intradermal genetic immunization by particle bombardment⁵. Here we present a non-viral gene-delivery system based on multisegment bimetallic nanorods that can simultaneously bind compacted DNA plasmids and targeting ligands in a spatially defined manner. This approach allows precise control of composition, size and multifunctionality of the gene-delivery system. Transfection experiments performed *in vitro* and *in vivo* provide promising results that suggest potential in genetic vaccination applications.

In this study we demonstrate the novel properties of bifunctional Au/Ni nanorods in gene transfer. Deposition of the nanorods was achieved by template synthesis, which involves electrochemical deposition into a non-conducting membrane having an array of cylindrical pores^{6,7}. Subsequent removal of the membrane by etching yields metallic nanorods of controlled dimensions. Template synthesis is advantageous because it is easily adapted for the deposition of multiple submicrometre segments. Furthermore, template synthesis can produce large quantities of monodisperse nanorods, and properties such as aspect ratio can be controlled in a systematic way.

The nanorods were fabricated⁸ by electrodeposition into an Al₂O₃ template (Anodisc, Whatman) with a pore diameter of 100 nm. An evaporated silver film on one side of the template served as the working electrode in a three-electrode configuration. A thin layer of silver was electrodeposited into the template from 50 mM KAg(CN)₂, 0.25 M Na₂CO₃ buffered to pH 13 at a potential of -1.0 V (Ag/AgCl) to ensure easy release of the nanorods from the template. The gold segments were deposited from a commercial gold-plating solution (Technic) at a potential of -1.0 V (Ag/AgCl), and the nickel segments were deposited from a solution of 20 g l⁻¹ NiCl₂·6H₂O, 515 g l⁻¹ Ni(H₂NSO₃)₂·4H₂O, 20 g l⁻¹ H₃BO₃ buffered to pH 3.4 at a potential of -1.0 V (Ag/AgCl). The silver layers were dissolved in 70 vol.% nitric acid and the alumina template was then dissolved in 2 M potassium hydroxide. The nanorods

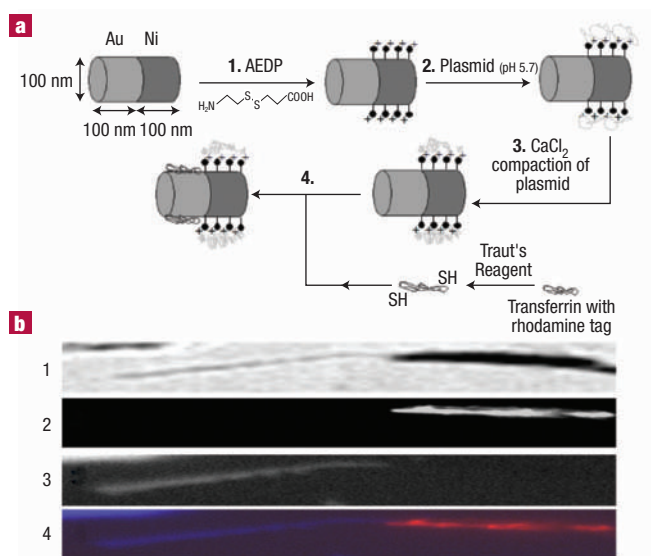


Figure 1 Spatially selective binding of DNA plasmids and transferrin to multicomponent nanorods. **a**, Illustration of nanorod functionalization. **1**, Nanorods are incubated with the 3-[(2-aminoethyl) dithio] propionic acid (AEDP) linker. The carboxylate end-group binds to the Ni segment. The disulphide linkage acts as a cleavable point within the spacer to promote DNA release within the reducing environment of the cell. **2**, Plasmids are bound by electrostatic interactions to the protonated amines presented on the surface of the nickel segment. **3**, CaCl₂ compacts the surface-immobilized plasmids. **4**, Rhodamine-conjugated transferrin is selectively bound to the gold segment of the nanorods. **b**, Confirmation of selective functionalization of nanorods is observed by light and fluorescent microscopy. **1**, Light microscope image of dual functionalized Au/Ni nanorod 20 μm long. **2**, Fluorescence image of the rhodamine-tagged (633 nm) transferrin on the Au segment. **3**, Fluorescence image of the Hoechst-stained (350/450 nm) plasmids on the Ni segment. **4**, Fluorescent overlay image combining **b2** and **b3**.

were washed repeatedly using 2 M potassium hydroxide, de-ionized water and ethanol. The nanorods were 100 nm in diameter and 200 nm in length with 100 nm gold segments and 100 nm nickel segments.

Using molecular linkages that bind selectively to either gold or nickel, we attached DNA and a cell-targeting protein, transferrin, to the different segments, as shown schematically in Fig. 1a. Transferrin is one of the first proteins exploited for receptor-mediated gene delivery, as all metabolic cells take in iron through receptor-mediated endocytosis of

were washed repeatedly using 2 M potassium hydroxide, de-ionized water and ethanol. The nanorods were 100 nm in diameter and 200 nm in length with 100 nm gold segments and 100 nm nickel segments.

Using molecular linkages that bind selectively to either gold or nickel, we attached DNA and a cell-targeting protein, transferrin, to the different segments, as shown schematically in Fig. 1a. Transferrin is one of the first proteins exploited for receptor-mediated gene delivery, as all metabolic cells take in iron through receptor-mediated endocytosis of

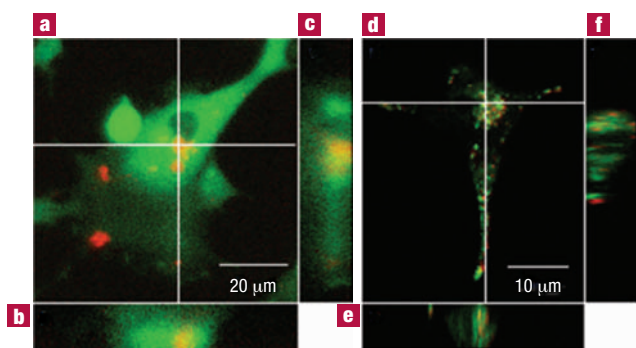


Figure 2 Stacked laser scanning confocal microscope images of transfected cells. **a**, A live HEK293 cell (red/633 nm, green/543 nm). Rhodamine (633 nm) identifies the subcellular location of the nanorods whilst GFP expression (543 nm) provides confirmation of transfection. **b, c**, Orthogonal sections confirm that the nanorods are within the cell. Confocal microscope stacked images **d**, of a live HEK 293 cell stained with LysoTracker Green identifying the location of the nanorods (Rhodamine) in relation to acidic organelles in both orthogonal sections **e** and **f**.

the transferrin–iron complex⁹. The transferrin was bound to the gold segments of the nanorods through a thiolate linkage¹⁰, by converting a small proportion of the primary amine groups of transferrin to sulphhydryl groups. A rhodamine tag on the transferrin provided a mechanism for confirmation of the presence of the nanorods in the cells and their intracellular distribution.

DNA was bound to the nickel segments by suspending the dual-component nanorods in a 0.1 M solution of 3-[(2-aminoethyl)dithio]propionic acid (AEDP). The carboxylic acid terminus of AEDP binds to the native oxide on the nickel segments. This resulted in the surface presentation of primary amine groups spaced by a reducible disulphide linkage. Plasmids encoding the 6.4 kb firefly luciferase (pCMV-luciferase VR1255_C) driven by the cytomegalovirus (CMV) promoter/enhancer (luciferase-plasmid), or plasmids encoding the GFPmut1 variant (pEGFP-C1) with 4.7 kb driven by the SV40 early promoter (GFP-plasmid), were conjugated to the AEDP bound to the nickel segments of the nanorods at pH 5.7. The surface plasmid concentration, determined from absorbance spectroscopy, was about 4×10^{12} molecules cm^{-2} .

To further compact the DNA bound to the nanorods for more efficient cell entry and protection of the DNA from enzymatic degradation, excess non-bound plasmids were removed and the nanorods were incubated in an aqueous solution of CaCl_2 for 24 hours. Ca^{2+} has a high affinity to DNA (having a dissociation constant, K_d of $1.1 \times 10^{-3} \text{M}^{-1}$), forming CaPO_4 complexes with the nucleic backbone to provide stabilization and compaction to the DNA structure¹¹.

Confirmation of the selective binding of transferrin and plasmid was obtained by fluorescence microscopy. As the 200-nm-long nanorods cannot be seen by optical microscopy, these experiments were performed on nanorods 20 μm long and 170 nm in diameter, having nickel and gold segments of equal length. Figure 1b shows uniform red fluorescence from the rhodamine-tagged transferrin on the gold segments and uniform blue fluorescence from the Hoechst stain (see Methods), which selectively binds to the DNA conjugated to the nickel segments.

To evaluate the gene-delivery potential of these dual-functionalized Au/Ni nanorods, *in vitro* transfection experiments were performed on the human embryonic kidney (HEK293) mammalian cell line with the GFP and luciferase reporter genes, respectively. For transfection, the nanorods were incubated with HEK293 cells for four hours in Opti-MEM

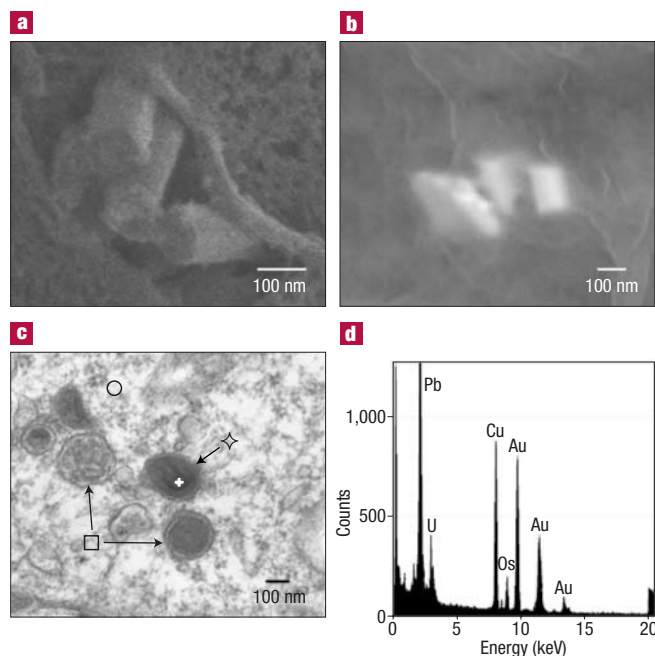


Figure 3 Uptake of nanorods observed by SEM and TEM analysis. **a**, SEM image of HEK293 cells after 1 h incubation with 200-nm Au/Ni nanorods. **b**, Back-scattered SEM image of 200-nm Au/Ni nanorods after 4 h incubation showing the nanorods beneath the surface of the cell. **c**, TEM cross-sectional image showing the presence of the nanorods in one of the vesicles (\diamond) after 4 h incubation; \circ denotes the cytoplasm of the cell and \square the empty vesicles. **d**, TEM-EDX spot analysis (white cross on Fig. 3c) providing confirmation that the nanorod is within the vesicle. The U, Pb, Cu and Os peaks are from grid and TEM sample preparation.

cell culture medium (Gibco BRL, Rockville, Maryland) at a dosing level ($44 \mu\text{ml}^{-1}$) significantly below the cytotoxicity or LD50 value (the dose lethal to 50% of cells) of the nanorods. This LD50 value as determined by the WST-1 assay was approximately $750 \mu\text{g ml}^{-1}$, which is about an order of magnitude less toxic than the $25 \mu\text{g ml}^{-1}$ LD50 value displayed by PEI (polyethyleneimine, branched and $M_w = 25,000$). Following washing, cells were further incubated in serum-containing media for two days. Figure 2a shows the characteristic green fluorescence from the GFP expressed by the cells as a result of transfection. Superimposed on the GFP emission is the red emission from the rhodamine conjugated to the Au segments of the nanorods. The orthogonal sections show clearly that the nanorods are located in the cell. Figure 2d shows fluorescence images from cells after 4 hours of incubation and stained with LysoTracker green, revealing that the nanorods are located in or around acidic organelles.

The uptake of the nanorods by HEK293 cells is shown in the scanning electron microscope (SEM) images in Fig. 3a,b after 1 and 4 hours of incubation, respectively. Transmission electron microscope (TEM) images and electron dispersive X-ray (EDX) analysis shows that the nanorods are located in the vesicles or the cytoplasm but not the nucleus. EDX spot analysis on the image of Fig. 3c shows the engulfment of the nanorods in one of the vesicles (Fig. 3c,d). This suggests that the transfection is due to plasmids released or cleaved from the nanorods prior to nuclear entry.

Figure 4 summarizes the results from a series of experiments undertaken to further characterize the transfection efficiency. Nanorods with compacted plasmids displayed a four-fold increase in GFP-positive cells in comparison with naked DNA. Luciferase expression by nanorod transfection was 255 times higher than that

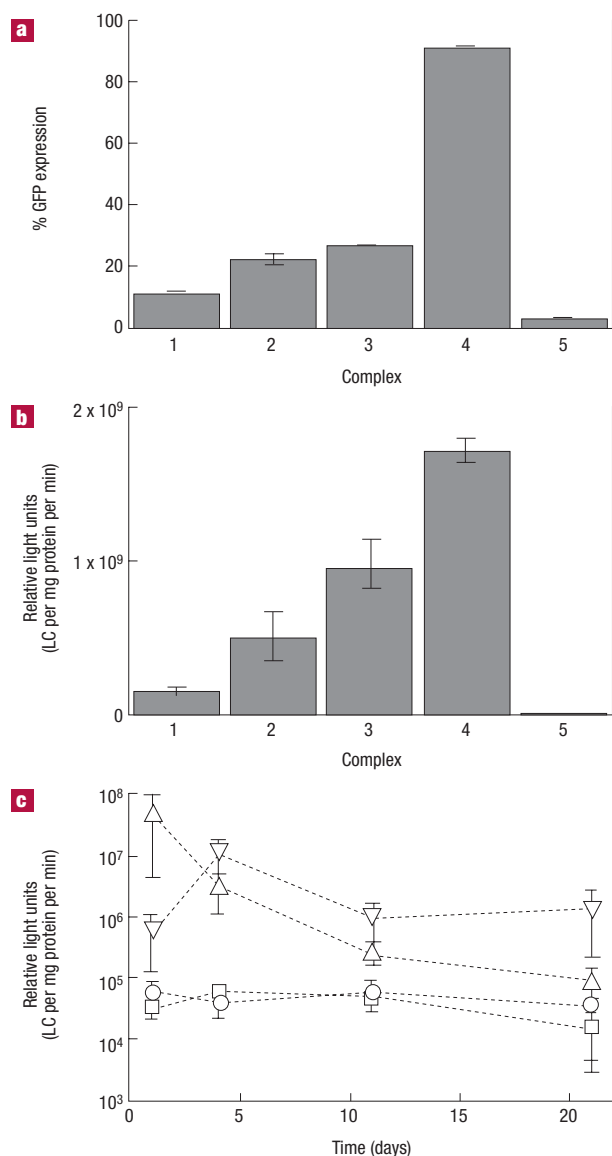


Figure 4 Results of transfection experiments. **a**, Histogram of percentage GFP expression (area of cells fluorescing/total cell area) and **b**, luciferase (LC) expression of **1**. nanorod–plasmid complex; **2**. nanorod–plasmid/transferrin complex; **3**. nanorod–plasmid/transferrin complex incubated with 100 μ M chloroquine; **4**. Lipofectamine (positive control); **5**. naked DNA (negative control). **c**, Plot of luciferase activity in skin and muscle of Balb/c mice. Legend: (Δ) intradermal-nanorods, (∇) intramuscular-nanorods, (\circ) intradermal-control and (\square) intramuscular-control.

mediated by naked DNA. Compared with nanorods with compacted plasmids alone, bifunctional nanorods conjugated with transferrin increased GFP expression by a factor of 2 (22%) and luciferase expression by a factor of 3.4. Further confirmation that transferrin was promoting receptor-mediated endocytosis of the nanorods was seen by an increase in GFP expression to 27% and increased luciferase expression by a factor of 1.9 in the presence of chloroquine in the cell culture medium. Chloroquine is an endosomolytic agent widely used to promote escape of the sequestered complexes from endosomal into cytoplasmic compartments⁴. Chloroquine may also enhance transfection by protecting against DNA degradation¹.

Preliminary *in vivo* efficacy studies (Fig. 4c) were performed in the skin and muscle tissues of mice. Delivery of the multicomponent nanorods to the skin was carried out using particle bombardment (Gene Gun), and delivery to the muscle was by injection. After one day, luciferase activity in the skin by nanorod transfection was 830 times higher than background (skin without nanorod delivery). The luciferase activity decreased after four days to approximately 80 times above background. Such transient expression would be suitable for genetic vaccination, where sustained transgene expression is not required. In contrast, intramuscular delivery of the nanorods resulted in only 17 times higher expression than the background after one day. However, the intramuscular luciferase activity was more prolonged, with a transgene expression level 85 times above background at day 21. Further optimization and toxicity studies will be necessary before the potential of these nanorods in systemic gene delivery can be established.

In summary, we have demonstrated a new approach for gene delivery using multisegment nanorods. Using molecules with end-groups that selectively bind to different metals, specific functionalities can be introduced to individual segments in the nanorod. Here we have used differential binding to attach plasmids and a cell-targeting protein to spatially separated regions of the delivery system. This approach can be extended to include other components that allow additional functionalities to be introduced. For example, an extra segment can be used to bind an endosomolytic agent or an external magnetic field can be used to manipulate nanorods with magnetic segments⁷. Thus, this versatile synthetic gene delivery system may help realize the potential of non-viral gene therapy.

METHODS

FUNCTIONALIZATION OF NANORODS

DNA binding: 150 μ l of 0.1 M AEDP (Pierce) solution was added to 200- μ l aliquots of nanorods ($\sim 1 \times 10^6$) suspended in distilled water. Following incubation for 24 h and washing, 2 μ g of plasmid was added to each aliquot of nanorods, (pH 5.7) and incubated at 4 $^{\circ}$ C for 24 h. After washing, 2 μ l of a 2 M CaCl_2 solution was added to each aliquot and then incubated for 24 h at 4 $^{\circ}$ C. For fluorescent staining of plasmids, nanorods were incubated with 100 μ l of 0.01 mg ml⁻¹ Hoechst 33258 (Bisbenzimidazole, Molecular Probes).

Transferrin binding: 5 mg of rhodamine-conjugated transferrin (Molecular Probes) in PBS with 5 mM EDTA was reacted with 120 μ l of 5 mg ml⁻¹ iminotriolane (Pierce) for 30 minutes at room temperature. The protein was purified by dialysis at 4 $^{\circ}$ C. 20 μ l of 5 mg ml⁻¹ rhodamine-transferrin-SH was added to each aliquot of nanorods and incubated for 24 h at 4 $^{\circ}$ C.

TRANSFECTION EXPERIMENTS

HEK293 cells (ATCC) were cultured in T75 flasks in DMEM (Dulbecco's modified Eagle's medium) supplemented with 10% fetal calf serum (FCS), 2 mM L-glutamine, 100 U ml⁻¹ penicillin, 100 μ g ml⁻¹ streptomycin and 0.25 μ g ml⁻¹ amphotericin B. All cell culture and Lipofectamine reagents were purchased from Gibco BRL, Rockville, Maryland. The serum-containing media was replaced every three days and split 1:3 at pre-confluence. The luciferase-encoded plasmids were a gift from Carl Wheeler, Vical. HEK293 cells were seeded onto 24-well plates (3×10^5 cells per well) for transfection using the luciferase plasmid, 12-well plates (8×10^5 cells per well) for transfection using the GFP-plasmid (Clontech) and 6-well plates (2×10^6 cells per well) for SEM and TEM studies. Each well (of the 24-well plate) was transfected in 0.5 ml reduced-serum Opti-MEM media (GIBCO). Selected wells were incubated with Opti-MEM containing 100 μ M chloroquine. Lipofectamine/DNA complexes at a ratio of 4:1 using 8 μ g Lipofectamine in 40 μ l Opti-MEM and 2 μ g DNA in 40 μ l Opti-MEM was added to control wells. 40 μ l of the nanorods/DNA suspension was added per well. After 4 h, the transfection media was removed and the cells washed. After three days of further incubation in serum-containing media, the wells were washed with phosphate-buffered saline (PBS) and imaged live. For confocal microscopy, chamber slides (Thomas Scientific, Swedesboro, New Jersey) were coated with 50 μ g ml⁻¹ collagen in 0.1 M acetic acid, washed with PBS and seeded with 5×10^4 cells. After 24 h, transfection was undertaken with GFP plasmid. For acidic organelle staining, HEK293 cells with nanorods were incubated with 75 nM LysoTracker Green (Molecular Probes) at 37 $^{\circ}$ C for 1 h in Opti-MEM media. Live HEK293 cells were viewed under a laser scanning confocal microscope (LSM 410, Carl Zeiss, USA). Transfection with the luciferase plasmid followed the same protocol for GFP plasmid with relative light units (RLU) measured using a luminometer (EG&G Berthold MiniLumat) and normalized to protein content using the BCA protein assay (Biorad). For SEM and TEM studies on uptake of the nanorods, cells were fixed with 2% glutaraldehyde/2% paraformaldehyde in PBS at selected time-points. After washing with PBS, cells were dehydrated with graded ethanol and coated with 2% osmium tetroxide (Aldrich). SEM samples were gold/platinum coated. SEM studies were performed on a JEOL 5600 LV. TEM samples were sectioned in epoxy resin by microtome and developed using 2% uranyl acetate and 0.04% lead citrate. TEM-EDX analysis was performed using a spot size of 5 nm with a Philips CM-300 FEG with EDX attachment. For *in vivo* studies, female Balb/c mice (Charles River Laboratories, Rockville, Maryland) were injected in the anterior tibialis muscle with 4 μ g DNA in 25 μ l nanorod solutions. For intradermal delivery by gene gun (Biorad, Hercules, California) the nanorods (4 μ g DNA) were applied to the shaved stomach of the

mice using 600 p.s.i. and following the Biorad protocol. The muscle and skin tissues were harvested, homogenized and assayed for luciferase activity at 1, 4, 11 and 21 days. All experiments were performed in quadruplicate.

Received 13 March 2003; accepted 4 August 2003; published 14 September 2003

References

1. Luo, D. & Saltzman, W. M. Synthetic DNA delivery systems. *Nature Biotechnol.* **18**, 33–37 (2000).
2. Roy, K., Mao, H. Q., Huang, S. K. & Leong, K. W. Oral gene delivery with chitosan-DNA nanoparticles generates immunologic protection in a murine model of peanut allergy. *Nature Med.* **5**, 387–391 (1999).
3. Carter, P. J. & Samulski, R. J. Adeno-associated viral vectors as gene delivery vehicles (review). *Int. J. Mol. Med.* **6**, 17–27 (2000).
4. Pouton, C. W. & Seymour, L. W. Key issues in non-viral gene delivery. *Adv. Drug Deliver. Rev.* **46**, 187–203 (2001).
5. Yang, N. S. & Sun, W. H. Gene gun and other nonviral approaches for cancer gene-therapy. *Nature Med.* **1**, 481–483 (1995).
6. Martin, C. R. Nanomaterials - a membrane-based synthetic approach. *Science* **266**, 1961–1966 (1994).
7. Whitney, T. M., Jiang, J. S., Searson, P. C. & Chien, C. L. Fabrication and magnetic-properties of arrays of metallic nanowires. *Science* **261**, 1316–1319 (1993).
8. Sun, L., Searson, P. C. & Chien, C. L. Magnetic anisotropy in prismatic nickel nanowires. *Appl. Phys. Lett.* **79**, 4429–4431 (2001).
9. Wagner, E., Curiel, D. & Cotten, M. Delivery of drugs, proteins and genes into cells using transferrin as a ligand for receptor-mediated endocytosis. *Adv. Drug Deliver. Rev.* **14**, 113–135 (1994).
10. Laibinis, P. E., Hickman, J. J., Wrighton, M. S. & Whitesides, G. M. Orthogonal self-assembled monolayers - alkanethiols on gold and alkane carboxylic-acids on alumina. *Science* **245**, 845–847 (1989).
11. Roy, I., Mitra, S., Maitra, A. & Mozumdar, S. Calcium phosphate nanoparticles as novel non-viral vectors for targeted gene delivery. *Int. J. Pharm.* **250**, 25–33 (2003).

Acknowledgements

This work was supported by the Defense Advanced Research Projects Agency (DARPA) and Air Force Office of Scientific Research (AFOSR, under grant number F49620-02-1-0307).

Correspondence and requests for materials should be addressed to K.W.L.

Competing financial interests

The authors declare that they have no competing financial interests.